Density-Functional-Theory-Based Study of the Dehydroxylation Behavior of Aluminous Dioctahedral 2:1 Layer-Type Clay Minerals

Stephen Stackhouse,*,† Peter V. Coveney,* and David M. Benoit

Centre for Computational Science, Department of Chemistry, University College London, Christopher Ingold Laboratories, 20 Gordon Street, London WC1H 0AJ, United Kingdom

Received: November 26, 2003; In Final Form: April 20, 2004

Density-functional calculations have been performed to investigate the mechanism of dehydroxylation in both *cis*- and *trans*-vacant pyrophyllite. In agreement with predictions from experiment, calculations show that both form a *trans*-vacant dehydroxylated structure, with aluminum in trigonal-bipyramidal coordination and a highly distorted tetrahedral layer. Differences in the dehydroxylation behavior of *cis*- and *trans*-vacant pyrophyllite are due to the fact that in the former, adjacent hydroxyl groups bridge different pairs of aluminum atoms, while in the latter they bridge the same pair. These conclusions are thought to be valid for all aluminous dioctahedral 2:1 layer type clay minerals.

1. Introduction

In general, clay minerals are layered materials composed of continuous two-dimensional silicate sheets stacked on top of each other in a well-defined manner. In the case of 2:1 clay minerals these sheets comprise a layer of metal ions in octahedral coordination sandwiched between two layers of linked silica tetrahedra.

The oxygen atoms supplied by the silica tetrahedra provide only two-thirds of the oxygen atoms necessary for the complete octahedral coordination of each metal ion. The remainder is supplied by hydroxyl groups that bridge two metal ions. The regular arrangement of the hydroxyl groups means that three distinct octahedral sites may be distinguished. These are designated cis or trans according to their position relative to the hydroxyls, as shown in Figure 1; two are cis and one is trans. When the metal ions present are divalent, such as in magnesium, all octahedral sites are filled and a *trioctahedral* sheet is obtained. However, when trivalent cations such as aluminum are present, just two out of three sites are occupied and a *dioctahedral* sheet is obtained. Incomplete filling of octahedral sites in dioctahedral sheets gives rise to the possibility of two structural isomers: one in which one cis and one trans site are occupied, defined as *cis*-vacant, and a second in which both cis cites are filled, known as *trans*-vacant.

The effect of thermal treatment on 2:1, dioctahedral clay minerals has been much studied by experimental methods.[1−3] These investigations have shown that three distinct behavioral phases are observed as the temperature is increased: (i) between 20 and 500 °C dehydration occurs—with increasing temperature water on the external surface, interlayer water hydrogen-bonded to the clay mineral layers, and interlayer water associated with metal counterions is lost; (ii) between 500 and 800 °C dehydroxylation occurs—structural hydroxyl groups react together and are lost as water; and (iii) between 800 and 1500 °C amorphization occurs—the dehydroxylated clay mineral structure decomposes into an amorphous phase. These temperature ranges vary with the type of clay mineral.

Of the three phases, dehydroxylation is both the most interesting and least well understood. Though some authors have studied the dehydroxylation behavior of a number of clay minerals, [4,5] the majority have focused on pyrophyllite[3,6−8] and montmorillonite.[1,2,9−18] In general, differential thermal analysis (DTA) or thermogravimetric analysis (TGA) have been used to monitor water loss during dehydroxylation, and infrared spectroscopy (IR) and X-ray diffraction (XRD) to follow structural changes in the clay minerals. In addition, some investigations have employed magic-angle-spinning nuclear magnetic resonance (MAS NMR) spectroscopic techniques to observe changes in ^{27}Al and ^{29}Si environments.[6−9]

Pyrophyllite is a *trans*-vacant, 2:1-layer-type clay mineral, characterized by no isomorphic substitution in either the octahedral or tetrahedral layer. It exhibits a dehydroxylation temperature of approximately 550 °C.[8] Prior to thermal treatment, ^{27}Al MAS NMR analysis shows a single sharp resonance due to aluminum in octahedral coordination, which disappears upon dehydroxylation as a more complex pattern assigned to aluminum in distorted trigonal-bipyramidal coordination emerges.[7,8] ^{29}Si MAS NMR analysis indicates that the silicate sheet layer structure is maintained upon dehydroxylation.[6,8] These observations have led to the postulation of a simple dehydroxylation mechanism for pyrophyllite—adjacent hydroxyl groups react to form water and a residual oxygen atom located in the plane of the aluminum atoms, where it experiences homogeneous charge compensation (Figure 2). This mechanism has recently been questioned by an infrared study, which reports evidence for a more complex two-stage process.[3] The authors conjectured that the process of pyrophyllite dehydroxylation is in fact a combination of dehydroxylation and rehydroxylation.

Montmorillonite is a *cis*-vacant,[19] 2:1-layer-type clay mineral characterized by partial substitution of aluminum by magnesium in the octahedral layer. The dehydroxylation temperature of most montmorillonites is about 700 °C,[4,5] but it has also been reported that for some dehydroxylation occurs in two stages, at 550 °C and again at 700 °C.[1,2] In addition, montmorillonites saturated

* Corresponding authors: s.stackhouse@ucl.ac.uk *p.v.coveney@ucl.ac.uk.

† Now based at the Department of Earth Sciences, University College London, Gower Street, London WC1E 6BT, United Kingdom.

10.1021/jp037608p CCC: $27.50
Published on Web 06/17/2004

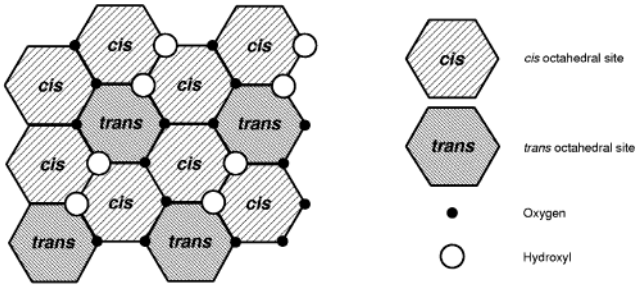

Figure 1. Schematic diagram of an octahedral sheet showing the different *cis*- and *trans* octahedral sites.

with different interlayer cations exhibit different dehydroxylation behavior.[13,15,18] Upon dehydration, small cations move into the ditrigonal cavities allowing the clay mineral layers to collapse to a greater extent than for larger cations, which remain in the interlayer holding them apart. Therefore, with small cations movement of water during dehydroxylation is diffusion controlled, whereas with larger cations first-order behavior is observed.[13] The type of interlayer cation is reported to have only a small effect on the activation energy of dehydroxylation,[13] with a value of about 250 kJ mol^{-1} calculated for Na^+, K^+, and Ca^{2+} saturated montmorillonites.

The mechanism for the dehydroxylation of montmorillonite is thought to be much more complex than that of pyrophyllite. Prior to thermal treatment ^{27}Al MAS NMR analysis shows a strong resonance due to aluminum in octahedral coordination and also a second much weaker resonance due to aluminum in tetrahedral coordination; upon dehydroxylation, the former disappears completely, while the latter remains largely unaffected.[9] Though no resonance assignable to five-coordinate aluminum has been observed for dehydroxylated montmorillonite, this is assumed to be due to use of a relatively weak magnetic field,[9] as compared to those employed to analyze dehydroxylation of pyrophyllite,[7,8] rather than its nonexistence.

Further insight into the dehydroxylation of montmorillonite has come from study of the rehydroxylated material. It has been shown that it is possible to rehydroxylate montmorillonite after dehydroxylation.[15−18] Investigations into the effect of thermal treatment on rehydroxylated montmorillonite have demonstrated that it exhibits a dehydroxylation temperature of approximately 550 °C,[5] which is 150 °C lower than that of the original clay mineral, more similar to that of pyrophyllite and other aluminous *trans*-vacant clay minerals.

In view of this, it has been postulated that upon dehydroxylation *cis*-vacant montmorillonite forms a *trans*-vacant dehydroxylated structure,[4,5] which upon rehydroxylation forms a *trans*-vacant clay mineral resembling pyrophyllite. This is corroborated by observations from X-ray diffraction studies of the dehydroxylation of other aluminous *cis*-vacant clay minerals,[4,5] which show similar behavior. The transformation not only explains the lower dehydroxylation temperature of rehydroxylated montmorillonite, but also provides a rationale for the fact that some montmorillonites—thought to comprise both *cis*- and *trans*-vacant layers—exhibit two different dehydroxylation temperatures.

The mechanism of dehydroxylation of montmorillonite is therefore suggested to proceed in two stages.[4,5] In the first, stage adjacent hydroxyl groups react to form water and a residual oxygen atom. The initial dehydroxylated structure is, however, calculated to be unstable, due to exceptionally long aluminum−oxygen bonds.[4,5] Stabilization is brought about by the migration of aluminum cations in trans sites to vacant cis sites. In this way the *cis*-vacant clay mineral forms a *trans*-vacant dehydroxylated structure (Figure 3).

The purpose of this paper is to examine the different dehydroxylation mechanisms of *cis*- and *trans*-vacant aluminous dioctahedral 2:1-layer-type clay minerals, using ab initio methods. In particular, we seek to understand the reason for the higher dehydroxylation temperature of *cis*-vacant clay minerals as compared to *trans*-vacant, which has been suggested to be due to the longer distance between adjacent hydroxyl groups in the former.[4, 5]

The paper is organized as follows. In Section 2 we describe the model systems and optimization methods used. This is followed by a presentation and discussion of the results of the calculations later in Section 3, starting with the optimized pyrophyllite structures and moving on to the calculated reaction energy profiles. In Section 4 we draw some conclusions.

2. Simulation Details

In this section we describe the model systems, methods used to perform the geometry optimization calculations and the geometric constraints applied.

2.1 Model Systems. The dehydroxylation-rehydroxylation behavior of aluminous dioctahedral 2:1-layer-type clay minerals with the same type of layers, that is, *cis*- or *trans*-vacant, has been shown to be similar, regardless of the type of isomorphic

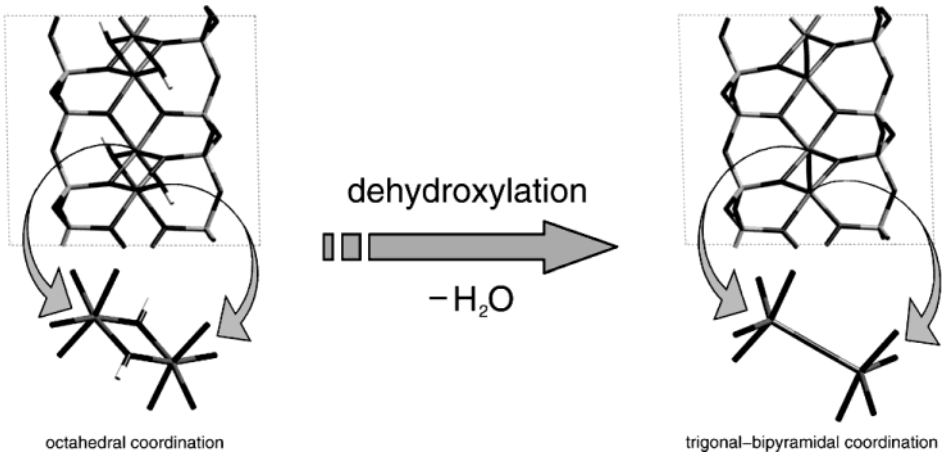

Figure 2. Proposed dehydroxylation of pyrophyllite−adjacent hydroxyl groups react to form water and a residual oxygen atom, which locates itself in the plane of the aluminum atoms, where it experiences homogeneous charge compensation. The color scheme here is white for hydrogen, black for oxygen, dark-gray for aluminum, and light-gray for silicon. Periodic boundaries are indicated by the dashed lines.

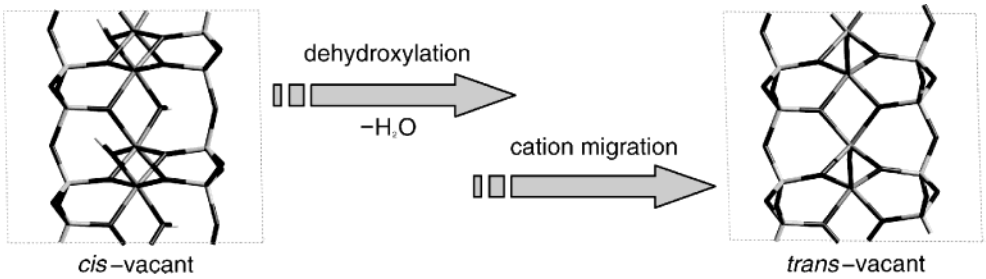

Figure 3. The dehydroxylation of montmorillonite is thought to proceed in two separate stages: (i) adjacent hydroxyl groups react to form water and a residual oxygen atom; (ii) aluminum cations in trans sites migrate to vacant cis sites. In this way the *cis*-vacant clay mineral forms a *trans*-vacant dehydroxylated structure. The color scheme here is white for hydrogen, black for oxygen, dark-gray for aluminum, and light-gray for silicon. Periodic boundaries are indicated by the dashed lines. Note that no magnesium-for-aluminum substitution is shown here.

substitution that they exhibit.[4,5] In addition, it is reported that the activation energy for the dehydroxylation of montmorillonite is predominantly dependent on the type of vacant sites in the octahedral layers and only to a small extent on the type of interlayer cations.[13] In view of this, and to keep the calculations simple, it was decided to study *cis*- and *trans*-vacant isomers of the charge-neutral clay mineral pyrophyllite, which exhibits neither isomorphic substitution nor interlayer cations.

Periodic models of *cis*- and *trans*-vacant pyrophyllite described in previous work,[20] each with unit cell formula $[Al_2(OH)_2Si_4O_{10}]_2$, were used as the initial models for the optimization calculations. The small size of the models was necessitated by the extremely large computational cost associated with electronic structure calculations.

2.2 Geometry Optimization. Geometry optimization calculations were carried out using the density-functional-theory based CPMD code,[21] which uses periodic boundary conditions and a planewave basis set. The CPMD code is very similar to the CASTEP code[22] used in previous work,[20] but allows much more complex geometric constraints to be applied during simulations. The exchange-correlation functional used adhered to the BLYP generalized gradient approximation,[23,24] ionic cores were described by Troullier-Martins norm-conserving pseudopotentials,[25] and the energy cutoff for the planewave expansion of the wave function was 120 Rydberg. The large size of the cell meant Brillouin zone sampling was restricted to the Γ- point.

Optimization of the wave function was achieved using the method of direct inversion in the interative subspace (DIIS),[26] while ionic positions were optimized using the Broyden-Fletcher-Goldfarb-Shanno (BFGS) algorithm[27] and cell parameters by steepest descents.[28]

In the planewave density functional method the number of planewaves required to represent a specified energy cutoff varies proportionally with the volume of the cell. In the CPMD prescription the necessary number of planewaves is calculated prior to optimization, based on the initial volume of the cell and kept constant throughout. This dictates that any variation in the volume of the cell during optimization causes the effective energy cutoff to deviate from the initial value; an increase in volume causes it to decrease, leading to a corresponding decrease in precision and vice versa. To imitate constant cutoff geometry optimization, an iterative scheme was adopted in which each cell was repeatedly reused until the change in the volume of the cell upon optimization was less than 1 Bohr.[3]

This scheme necessitated the use of a very high energy cutoff, to reduce to an acceptable level unphysical discontinuities in the total energies of the model systems, associated with the change in the number of planewaves required to represent the wave function, at different cell volumes. Preliminary calculations showed that, for an energy cutoff of 120 Rydberg, these discontinuities were reduced to approximately 0.25 kJ mol^{-1}, which was considered an acceptable limit in the present study where activation energies were expected to be in the hundreds of kilojoules per mole.

2.3 Geometric Constraints. The *cis*- and *trans*-vacant pyrophyllite models were initially optimized with no atom or cell constraints applied. To simulate the process of dehydroxylation they were then reused with a series of different geometric constraints applied.

Two types of dehydroxylation were investigated: (i) *partial dehydroxylation*, in which just one pair of adjacent hydroxyl groups was constrained to react and form a water molecule; and (ii) *total dehydroxylation*, in which both pairs of adjacent hydroxyl groups were constrained to react and form water molecules. The periodic nature of the models meant that the former corresponded to the simultaneous reaction of alternate pairs of adjacent hydroxyl groups and the latter to the simultaneous reaction of all pairs of adjacent hydroxyl groups. Though neither is an exact representation of the dehydroxylation process, they were considered the most useful, tractable calculations.

In each case the dehydroxylation process was simulated in two separate stages: (i) The first is *protonation*—protonation of hydroxyl group(s) by adjacent hydroxyl group(s). This was achieved by successive reoptimization of each model with the distance between the oxygen atom of one hydroxyl group and the proton of the adjacent hydroxyl group constrained at a progressively shorter distance. (ii) The second is *water migration*—migration of water molecule(s) formed by protonation into the interlayer. This was achieved by successive reoptimization of each model with the distance between the oxygen atom of the water molecule and a dummy atom near the center of the closest hexagonal ring constrained at a progressively shorter distance. More specific details are provided in Table 1. Note that the final model from the protonation stage was used as the initial model for the water migration stage.

In addition, completely dehydroxylated structures were created by removing the water molecules from the *cis*- and *trans*-vacant pyrophyllite models that had undergone the process of total dehydroxylation. These were optimized with no atom or cell constraints applied.

3. Results and Discussion

In this section we discuss the results of our simulations. We begin with details of the optimized periodic *cis*- and *trans*-vacant pyrophyllite structures. This is followed by the energy profiles for the partial and total dehydroxylation of both models.

3.1 Optimized Structures. Figures 4 and 5 show the optimized *cis*- and *trans*-vacant pyrophyllite models, before and

TABLE 1: Geometric Constraints Applied to Pyrophyllite Models to Promote Dehydroxylation

process	constraint(s) applied[a,b,c]	
partial dehydroxylation of *cis*-vacant pyrophyllite	protonation[d] O9−H2 = 2.700 Å → 0.991 Å	water migration D(O20, O21, O22)−O9 = 2.400 Å → 0.000 Å; O9−H2 < 1.000 Å
partial dehydroxylation of *trans*-vacant pyrophyllite	protonation[e] O8−H1 = 2.900 Å → 1.310 Å	water migration D(O19, O20, O21)−O9 = 1.200 Å → 0.000 Å
total dehydroxylation of *cis*-vacant pyrophyllite	protonation[d] O9−H2 = 2.700 Å → 0.991 Å; O12−H1 = 2.700 Å 0.991 Å	water migration D(O20, O22) = 2.600 Å → 1.000 Å; D(O19, O23)−O12 = 2.600 Å → 1.000 Å; O9−H2 < 1.000 Å; O12−H1 < 1.000 Å
total dehydroxylation of *trans*-vacant pyrophyllite	protonation[e] O8−H1 = 2.900 Å → 1.260 Å; O11−H3 = 2.900 Å → 1.260 Å	water migration D(O19, O21)−O8 = 1.700 Å → 1.000 Å; D(O22, O24)−O11 = 1.700 Å → 1.000 Å

[a] Atom labels refer to Figures 4 and 5. [b] X1−X2 = N1 → N2 indicates that the distance between atoms X1 and X2 was constrained at N1 and progressively lower values until a value of N2 was reached. [c] D(X1, X2...) indicates a dummy atom located at the arithmetic mean of the coordinate of atoms X1, X2... [d] 0.991 Å is the calculated average O−H bond length for liquid water, using a similar density functional method to that used in this work.[29] [e] In the case of the *trans*-vacant pyrophyllite models protonation was spontaneous once the proton was brought within a specific distance of the oxygen atom.

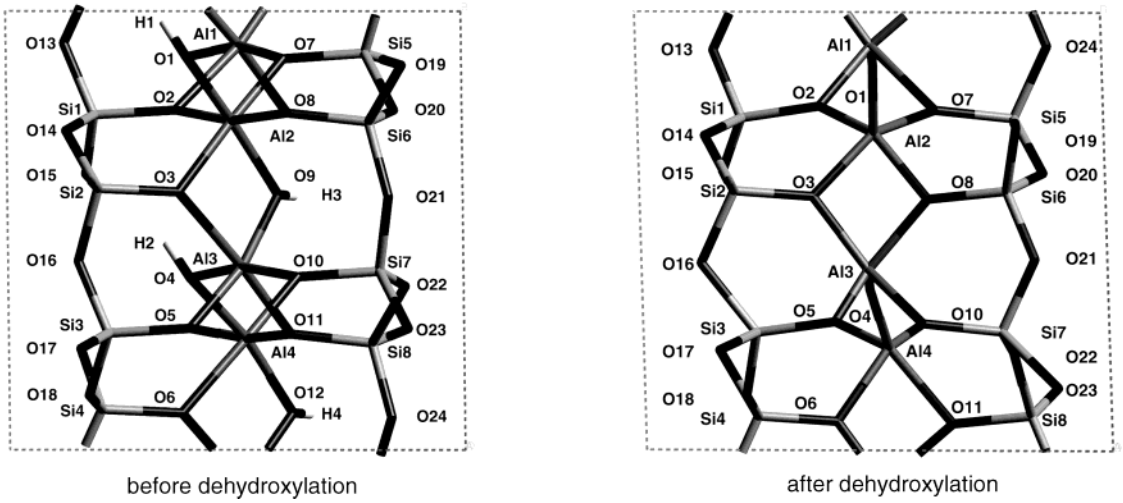

Figure 4. Optimized *cis*-vacant pyrophyllite model. The color scheme here is white for hydrogen, black for oxygen, dark-gray for aluminum, and light-gray for silicon. Periodic boundaries are indicated by the dashed lines.

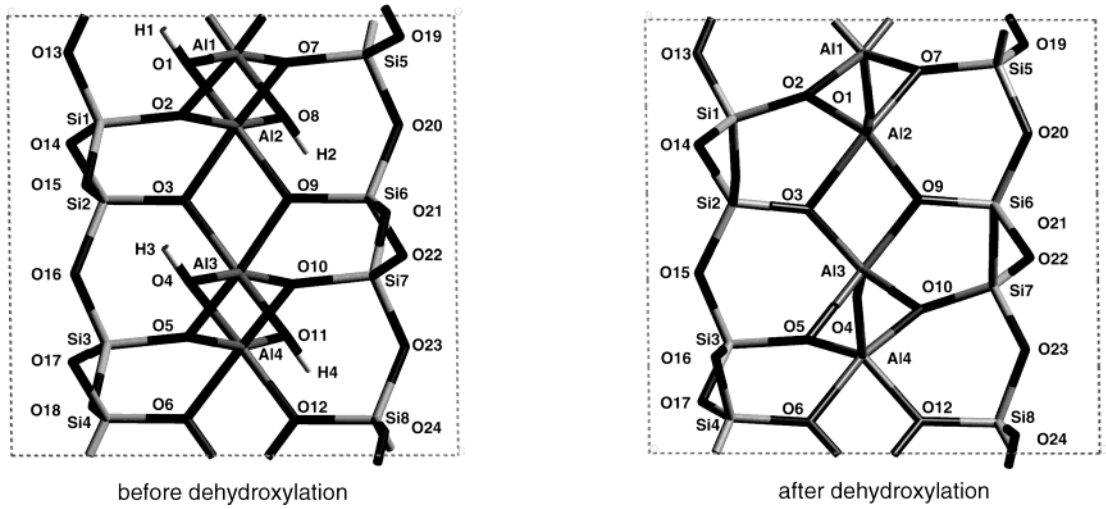

Figure 5. Optimized *trans*-vacant pyrophyllite model. The color scheme here is white for hydrogen, black for oxygen, dark-gray for aluminum, and light-gray for silicon. Periodic boundaries are indicated by the dashed lines.

after dehydroxylation. The atom labels are consistent for each isomer, going from before to after dehydroxylation, so that movement of atoms can be traced.

One can see that the *cis*- and *trans*-vacant pyrophyllite models both form a similar *trans*-vacant structure upon dehydroxylation, as postulated by Drits et al.[4,5] In both dehydroxylated structures the residual oxygen atoms reside within the plane of the aluminum atoms, as proposed by Drits et al. [4,5] and in agreement with the crystal structure of dehydroxylated *trans*-vacant pyrophyllite determined by X-ray diffraction methods.[30] In addition, all aluminum atoms exhibit distorted trigonal-bipyramidal coordination in good accord with observations from ^{27}Al MAS

TABLE 2: Unit Cell Parameters and Volumes of Optimized Pyrophyllite Models; Lengths Are in Å, Angles Are in Degrees, and Volumes in Å^3

clay structure	a	b	c	α	*β*	*γ*	vol.
cis-vacant pyrophyllite	5.288	9.232	9.662	89.29	98.65	90.07	466.3
cis-vacant montmorillonite[a]	5.193	8.994					
dehydroxylated *cis*-vacant pyrophyllite	5.214	9.427	10.26	87.57	103.5	92.16	489.5
dehydroxylated *cis*-vacant pyrophyllite[a]	5.241	9.078					
trans-vacant pyrophyllite	5.306	9.261	9.561	90.51	100.4	89.69	462.1
trans-vacant pyrophyllite[b]	5.161	8.957	9.351		100.4		
Dehydroxylated *trans*-vacant pyrophyllite	5.248	9.430	9.972	91.02	101.0	87.73	484.0
dehydroxylated *trans*-vacant pyrophyllite[b]	5.192	9.122	9.499		100.2		

[a] Experimental values from Mullet et al.[5] [b] Experimental values from Drits et al.[4]

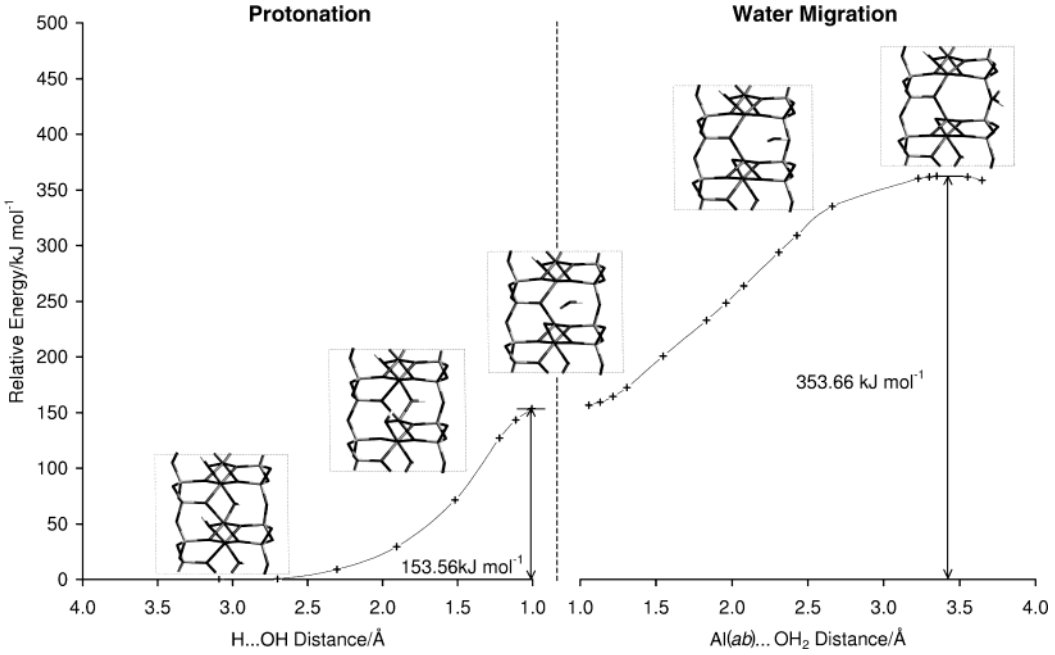

Figure 6. Energy profile for partial dehydroxylation of the *cis*-vacant pyrophyllite model. The color scheme here is white for hydrogen, black for oxygen, dark-gray for aluminum, and light-gray for silicon.

NMR studies.[7−9] It is also noticeable that the silicate network of the tetrahedral layers is distorted as compared to the initial models, the Si−O−Si angles of the structure derived from *cis*-vacant pyrophyllite in particular. This is consistent with observations from ^{29}Si MAS NMR-[3,6,8] and IR-based[13] investigations.

The unit cell parameters of the optimized pyrophyllite models are listed in Table 2 with corresponding experimental data also presented for comparison. In general, calculated unit cell lengths are slightly longer than experimental values, while angles are in reasonable agreement. The most noticeable change in the calculated unit cell parameters, upon dehydroxylation, is the large increase in *b*, which is observed experimentally, but to a much lesser extent. The small increase in *a* observed experimentally is not seen in the calculated values. These differences are most likely due to the small size of the models. The unit cell volumes of the optimized pyrophyllite models are also reported in Table 2. These indicate that upon dehydroxylation the unit cell volume of both *cis*- and *trans*-vacant pyrophyllite increases by about 23 Å,^{3} due to the increase in *b* and *c*, in agreement with experiment.

It has been postulated that the higher dehydroxylation temperature of *cis*-vacant aluminous dioctahedral 2:1-layer-type clay minerals, as compared to similar *trans*-vacant clay minerals, is predominantly due to the longer distance between adjacent hydroxyl groups in the former.[4] This is based on the assumption that the thermal energy required for the proton of one hydroxyl group to transfer to the oxygen atom of an adjacent hydroxyl group is primarily dependent on the distance between the two. It is very likely, however, that this conclusion was reached on the basis of hydroxyl oxygen atom positions only.

In the optimized *cis*-vacant pyrophyllite model, the average distance between the oxygen atoms of adjacent hydroxyl groups is 2.822 Å, while in the optimized *trans*-vacant pyrophyllite model it is 2.420 Å. This is in agreement with experiment. Note, however, that the average distance between the proton of a hydroxyl group and the oxygen atom of an adjacent hydroxyl group is only 2.953 Å in the *cis*-vacant pyrophyllite model, but significantly larger at 3.311 Å, in the *trans*-vacant model. This implies that some factor other than proximity of adjacent hydroxyl groups is responsible for the difference in dehydroxylation temperatures.

3.2 Dehydroxylation Reaction Energy Profiles. Figures 6, 7, 8, and 9 show the energy profiles for the four dehydroxylation reactions investigated. These are also plotted together in Figure 10 in order to aid their comparison. Each comprises a protonation and water migration stage. In the protonation stage the relative energy of the system is plotted against the distance between the approaching proton and the accepting oxygen atom, while in the water migration stage it is plotted against the distance between the water oxygen atom and the plane through the center of the aluminum atoms. The protonation stage will be discussed separately first, followed by the water migration stage.

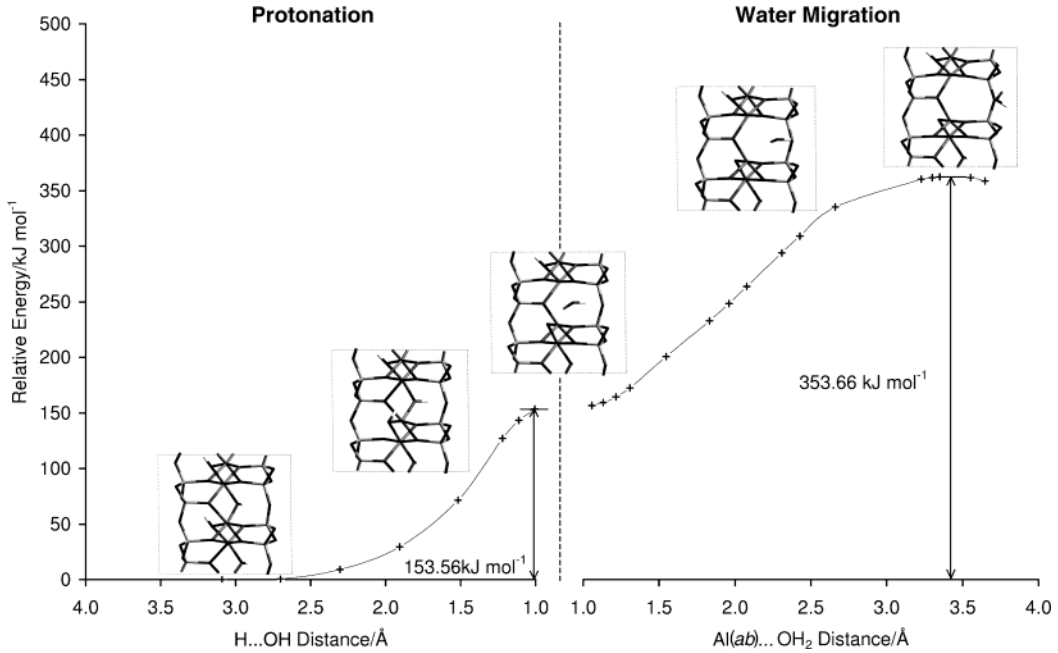

Figure 7. Energy profile for partial dehydroxylation of the *trans*-vacant pyrophyllite model. The color scheme here is white for hydrogen, black for oxygen, dark-gray for aluminum, and light-gray for silicon.

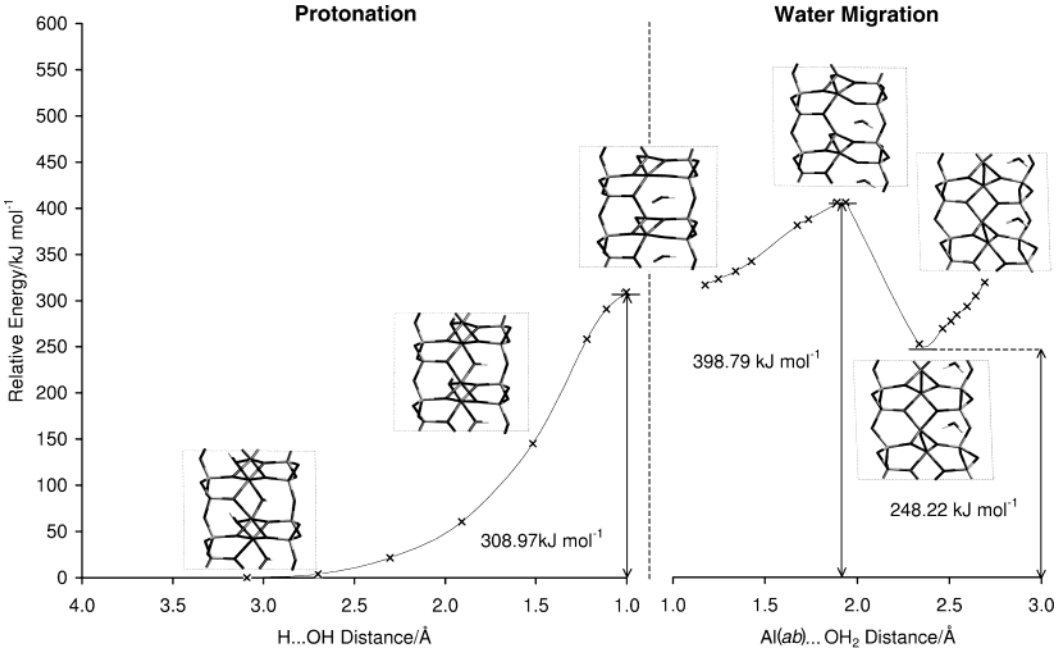

Figure 8. Energy profile for total dehydroxylation of the *cis*-vacant pyrophyllite model. The color scheme here is white for hydrogen, black for oxygen, dark-gray for aluminum, and light-gray for silicon.

The reaction energy profiles for the partial and total dehydroxylation of the *cis*-vacant pyrophyllite model are shown in Figures 6 and 8. These indicate that in *cis*-vacant pyrophyllite the energy required for a hydroxyl group to protonate an adjacent hydroxyl group, forming a water molecule, is about 155 kJ mol^{-1}. Note that for total dehydroxylation two protonation reactions occur simultaneously; the energy required for one is thus equal to half that for the whole protonation stage. The form of the energy profiles implies, however, that a water molecule formed by such a reaction is unstable toward dissociation and reformation of the original hydroxyl groups, that is, rehydroxylation.

The reaction energy profiles for the partial and total dehydroxylation of the *trans*-vacant pyrophyllite model are shown in Figures 7 and 9. In both cases it was only necessary to constrain the proton to approach the oxygen atom up to a distance of about 1.3 Å. Once in such proximity, the models were optimized without constraints, upon which protonation was observed to occur spontaneously, forming a water molecule, which rested in a ditrigonal cavity. These structures correspond to the first points in the water migration stages. Thus, in *trans*-vacant pyrophyllite the energy required for a hydroxyl group to protonate an adjacent hydroxyl group is equal to the energy necessary to bring the proton within about 1.3 Å of the oxygen atom, shown to be approximately 235 kJ mol^{-1}.

These results indicate not only that the energy required to enable a hydroxyl group to protonate an adjacent hydroxyl group is much less in *cis*-vacant pyrophyllite, as compared to *trans*-vacant, but also that a water molecule formed by such a reaction in *cis*-vacant pyrophyllite is unstable toward rehydroxylation,

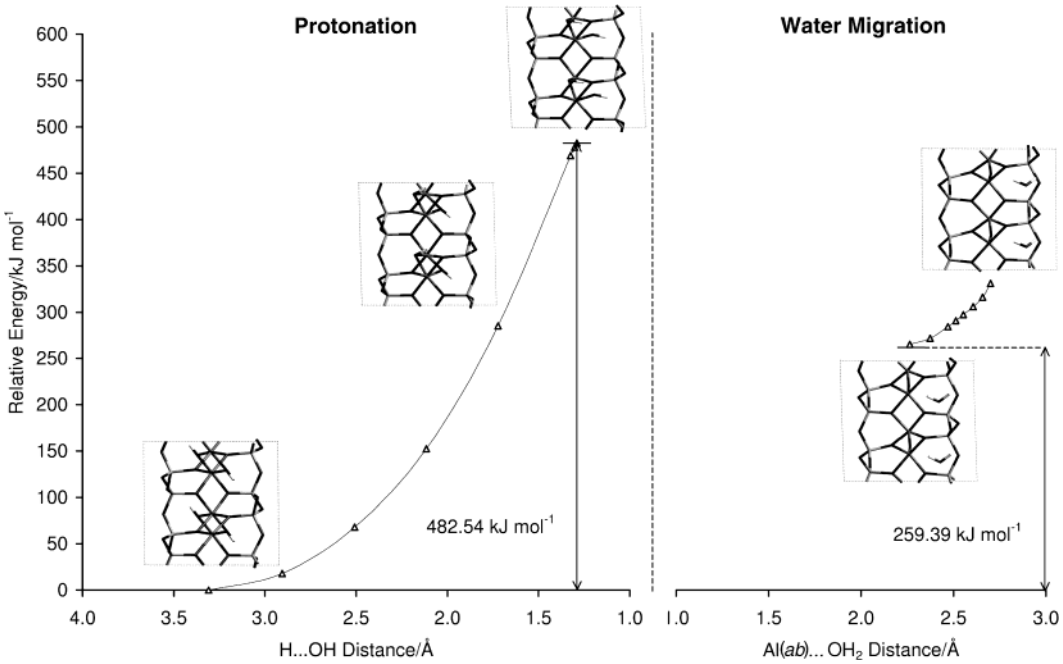

Figure 9. Energy profile for total dehydroxylation of the *trans*-vacant pyrophyllite model. The color scheme here is white for hydrogen, black for oxygen, dark-gray for aluminum, and light-gray for silicon.

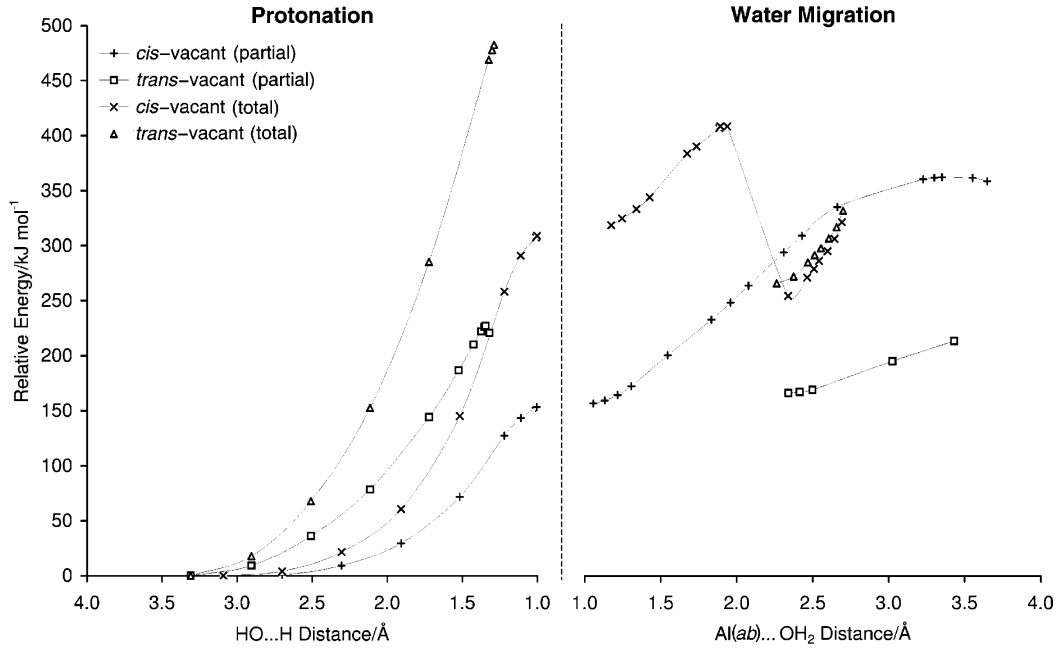

Figure 10. Energy profile for all dehydroxylation reactions.

while in *trans*-vacant, once formed, a water molecule is relatively stable.

To understand these results one must consider the subtle differences in the structures of the isomers. In particular, the fact that in *cis*-vacant pyrophyllite adjacent hydroxyl groups bridge different pairs of aluminum atoms, whereas in *trans*-vacant pyrophyllite they are both bonded to the same pair.

It was noted in the previous section that although the distance between adjacent hydroxyl oxygen atoms is greater in *cis*-vacant pyrophyllite, as compared to *trans*-vacant pyrophyllite, the distance between the proton of a hydroxyl group and the oxygen atom of an adjacent hydroxyl group is shorter. It could therefore be postulated that the lower energy required to bring about protonation in *cis*-vacant pyrophyllite, as compared to *trans*-vacant pyrophyllite, is due to the shorter distance the proton must travel. In fact, in both isomers the distance between the proton of a hydroxyl group and the oxygen atom of an adjacent hydroxyl group is too large for the proton to jump across. For protonation to occur, it is necessary for the hydroxyl oxygen atoms to rearrange and the hydroxyl bonds to reorient, to bring them into closer proximity.

In *cis*-vacant pyrophyllite the distance between adjacent hydroxyl oxygen atoms is approximately 2.8 Å, while that between the proton of a hydroxyl group and the oxygen atom of an adjacent hydroxyl group is approximately 2.9 Å. The simulations show that during protonation, adjacent hydroxyl oxygen atoms move to within approximately 2.3 Å. In addition, the hydroxyl bonds reorient. Consequently, at the instant proton transfer begins the distance between the proton and the adjacent oxygen atom is approximately 1.2 Å. The important point to

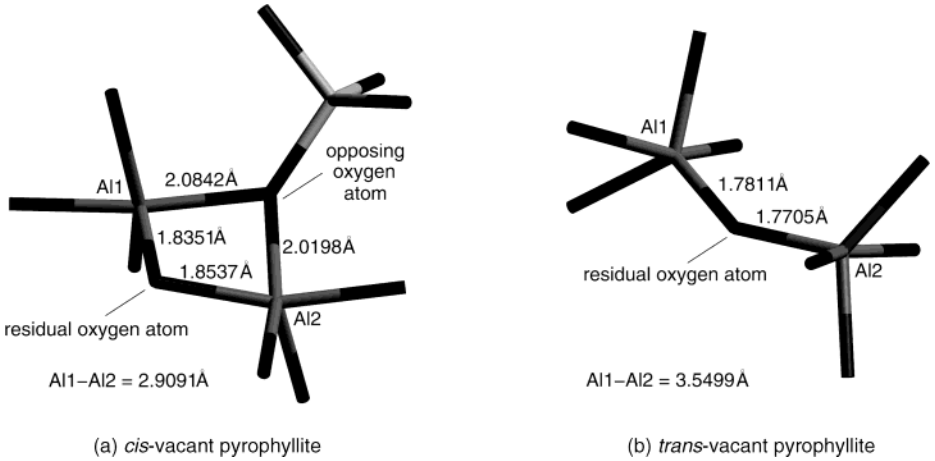

(a) *cis*-vacant pyrophyllite (b) *trans*-vacant pyrophyllite

Figure 11. Fragments from optimized *cis*- and *trans*-vacant pyrophyllite models showing the location of residual oxygen atoms immediately after protonation. The color scheme here is black for oxygen, dark-gray for aluminum, and light-gray for silicon.

note is that the rearrangement of the hydroxyl oxygen atoms and reorientation of the hydroxyl bonds is relatively sterically unhindered, because the hydroxyl groups bridge different pairs of aluminum atoms.

In *trans*-vacant pyrophyllite the distance between adjacent hydroxyl oxygen atoms is approximately 2.4 Å, while that between the proton of a hydroxyl group and the oxygen atom of an adjacent hydroxyl group is approximately 3.3 Å. The simulations show that during protonation, adjacent hydroxyl oxygen atoms move to within approximately 2.2 Å. In addition, the hydroxyl bonds reorient, with one rotating up to 180°. Consequently, at the instant proton transfer begins the distance between the proton and the adjacent oxygen atom is approximately 1.3 Å. These rearrangements are, however, highly sterically hindered, due to the fact that adjacent hydroxyl groups bridge the same pair of aluminum atoms. This not only constrains the relative movement of the hydroxyl oxygen atoms, but also prescribes that hydroxyl bonds orient in opposing directions.

In view of this, we conclude that the lower energy required to induce protonation in *cis*-vacant pyrophyllite, as compared to *trans*-vacant pyrophyllite, is due to the lower energy necessary for the rearrangement of the hydroxyl oxygen atoms and reorientation of hydroxyl bonds. This is due to the fact that, in *cis*-vacant pyrophyllite, adjacent hydroxyl groups bridge different pairs of aluminum atoms, whereas in *trans*-vacant pyrophyllite they are both bonded to the same pair.

The same structural difference is also responsible for the different stabilities of water molecules, formed by hydroxyl protonation, in the two isomers. When one hydroxyl group protonates another, a water molecule and residual oxygen atom are formed. It can be seen in the dehydroxylation energy profiles of both isomers that, as protonation proceeds, the residual oxygen atoms move toward the plane of the aluminum atoms, in an attempt to obtain uniform charge compensation.

It is apparent from Figures 6 and 8 that in *cis*-vacant pyrophyllite residual oxygen atoms are unable to move fully into the plane of the aluminum atoms (unless cation migration occurs). This is because of an opposing oxygen atom, which bridges the same pair of aluminum atoms, illustrated in Figure 11(a). The opposing oxygen atom, as part of the tetrahedral layer, is fixed in position and inhibits movement of the residual oxygen atom between the aluminum atoms. It is seen in Figures 6 and 8 that this causes the residual oxygen atom to be insufficiently charge-compensated by the aluminum atoms, which makes it extremely susceptible to reprotonation by the associated water molecule. The water molecule is inhibited from moving away, into a ditrigonal cavity, since it must balance the asymmetric charge distribution around the aluminum atoms, generated by the ill-positioned residual oxygen atom. The combination of these factors renders the water molecule unstable toward rehydroxylation.

In contrast, Figures 7 and 9 show that in *trans*-vacant pyrophyllite residual oxygen atoms are able to move into the center of the plane of the aluminum atoms. With adjacent hydroxyl groups bridging the same pair of Al atoms, one of the two oxygen atoms on protonation gets incorporated into a water molecule that is relatively free to move within the clay matrix. It can be seen in Figures 7 and 9 that, in *trans*-vacant pyrophyllite protonation, movement of the residual oxygen atom into the plane of the aluminum atoms and expulsion of the water molecule formed into a ditrigonal cavity indeed occur concurrently. When the water molecule moves into a ditrigonal cavity, the residual oxygen atom can move fully into the center of the plane of the aluminum atoms. This leads to a decrease in aluminum−oxygen and an increase in aluminum−aluminum bond lengths, as seen in Figure 11(b). The overall process results in uniform charge compensation for the residual oxygen and aluminum atoms and, consequently, a stable water molecule.

In view of this, it is concluded that a water molecule formed by the reaction of two hydroxyl groups in *cis*-vacant pyrophyllite is unstable toward rehydroxylation, because the residual oxygen atom is unable to move fully into the center of the plane of the aluminum atoms, resulting in an unfavorable separation of charge. In *trans*-vacant pyrophyllite, however, the residual oxygen atom is able to move into the center of the plane of the aluminum atoms, leading to homogeneous charge compensation and a stable water molecule. These differences originate from the fact that in *cis*-vacant pyrophyllite adjacent hydroxyl groups bridge different pairs of aluminum atoms, whereas in *trans*-vacant pyrophyllite they bridge the same pair.

We now turn our attention to the water migration stage of the dehydroxylation energy profiles. These show the energetics of the systems as water molecules migrate across the ditrigonal cavity toward the interlayer. It will be seen that this is very different for each of the isomers.

The energy profile for the partial dehydroxylation of *cis*-vacant pyrophyllite is shown in Figure 6. It can be seen that it is extremely unfavorable for the water molecule to move across the ditrigonal cavity toward the interlayer. This is due to the fact that as the water molecule migrates it is less able to compensate the asymmetric charge distribution caused by the

residual oxygen atom. If one considers the whole profile, it is clear that the water molecule is unstable toward rehydroxylation up until the point at which it exits the ditrigonal cavity. The energy barrier to this is in the region of 200 kJ mol^{-1}. If added to the activation energy for protonation, it gives a total activation energy for dehydroxylation of approximately 350 kJ mol^{-1}. Note, however, that cation migration does not occur.

The energy profile for the partial dehydroxylation of *trans*-vacant pyrophyllite is shown in Figure 7. It can be seen that although it is unfavorable for the water molecule to move across the ditrigonal cavity toward the interlayer, it is so to a much lesser extent than that observed in the partial dehydroxylation of the *cis*-vacant isomer. This is because the residual oxygen and aluminum atoms are homogeneously charge-compensated and it is therefore predominantly steric, as opposed to coloumbic, interactions that hinder migration of the water molecule. In contrast to the *cis*-vacant case, the energy profile shows that the water molecule is always stable toward rehydroxylation during migration to the interlayer. The energy barrier to complete expulsion is approximately 50 kJ mol^{-1}, which is four times smaller than that calculated in the partial dehydroxylation of the *cis*-vacant isomer. The activation energy for dehydroxylation is simply equal to that for protonation, calculated to be approximately 230 kJ mol^{-1}.

The energy profile for the total dehydroxylation of *cis*-vacant pyrophyllite is shown in Figure 8. It can be seen that it is initially extremely unfavorable for the two water molecules to move across the ditrigonal cavity toward the interlayer. The energy barrier is similar to that observed in the partial dehydroxylation of the same isomer. Things change dramatically, however, as the water molecules migrate further and are less able to compensate the asymmetric charge distribution around the aluminum atoms. Once the water molecules are a certain distance from the plane of the aluminum atoms the coloumbic interactions between the residual oxygen atoms and aluminum atoms become so acutely unfavorable that cation migration occurs. This results in a *trans*-vacant structure, wherein the residual oxygen atoms and aluminum atoms are uniformly charge-compensated, and incurs a gain in energy of about 150 kJ mol^{-1}. Thereafter the water molecules experience an energy barrier to migration similar to that observed in the total and partial dehydroxylation of the *trans*-vacant isomer, seen in Figure 10. The total activation energy for dehydroxylation is approximately 200 kJ mol^{-1}, which is that required to bring about protonation and induce cation migration.

The energy profile for the total dehydroxylation of *trans*-vacant pyrophyllite is shown in Figure 9. It can be seen that again it is unfavorable for the water molecules to move across the ditrigonal cavity towards the interlayer. The energy barrier is similar to that observed in the partial dehydroxylation of the same isomer. The activation energy for dehydroxylation is likewise equal to that for protonation, calculated to be approximately 240 kJ mol^{-1}.

If we compare the activation energies for the dehydroxylation of *cis*-vacant pyrophyllite calculated from the partial and total dehydroxylation reactions we find that they are very different. The value calculated from partial dehydroxylation is approximately 350 kJ mol^{-1}, which is significantly larger than the 200 kJ mol^{-1} deduced from total dehydroxylation. This is because of the occurrence of cation migration in the total dehydroxylation case, which as discussed above, reduces the energy barrier toward the water molecules migrating to the interlayer.

We postulate that in order for cation migration to occur in *cis*-vacant pyrophyllite a large number of neighboring pairs of adjacent hydroxyl groups must react, so as to introduce sufficient flexibility into the layer structure. This accounts for why it is not observed in the partial dehydroxylation case, but is seen for total dehydroxylation. Based on this assumption, dehydroxylation may proceed in two ways. In the first scenario, pairs of adjacent hydroxyl groups react in a sequential manner, with an associated activation energy similar to that calculated from the partial dehydroxylation case. But, as this continues more flexibility is introduced into the layer structure; cation migration becomes more prevalent and the activation energy for dehydroxylation of further pairs of adjacent hydroxyl groups decreases. In the second scenario, large numbers of neighboring pairs of adjacent hydroxyl groups react together simultaneously, with an associated activation energy similar to that calculated for the total dehydroxylation case. In fact, we believe that a combination of both dehydroxylation mechanisms is most likely: it would lead to an activation energy for dehydroxylation between the two calculated values, and one closer to the 250 kJ mol^{-1} determined by experiment for montmorillonite.[13]

Evidence for this kind of dehydroxylation behavior in *cis*-vacant pyrophyllite has been observed in experimental studies. It has been reported that using a slower heating rate during thermal treatment reduces the dehydroxylation temperature of montmorillonite samples.[16] We suggest that using a slower heating rate causes larger numbers of pairs of adjacent hydroxyl groups to simultaneously acquire the energy to react together. Dehydroxylation would therefore proceed via the second mechanism, with the lower associated activation energy.

In contrast, the activation energies for dehydroxylation of *trans*-vacant pyrophyllite calculated from the partial and total dehydroxylation reactions are almost exactly the same at approximately 235 kJ mol^{-1}. This implies that in *trans*-vacant pyrophyllite the activation energy for dehydroxylation of each pair of adjacent hydroxyl groups is the same and independent of the dehydroxylation state of neighboring pairs.

Although our calculations have only been concerned with pyrophyllite it is not unreasonable to expect our conclusions to be applicable to other aluminous dioctahedral 2:1-layer-type clay minerals, since they are observed, by experiment, to exhibit very similar dehydroxylation behavior.[4,5]

4. Conclusions

Upon dehydroxylation, *cis*- and *trans*-vacant pyrophyllite form the same *trans*-vacant structure, with aluminum in trigonal bipyramidal coordination and a highly distorted tetrahedral layer. The energy required to enable a hydroxyl group to protonate an adjacent hydroxyl group is much less in *cis*-vacant pyrophyllite, as compared to *trans*-vacant pyrophyllite, but a water molecule formed by such a reaction in the former is unstable towards rehydroxylation, while in the latter, once formed, a water molecule is relatively stable. In order for water molecules to be stable toward rehydroxylation, in *cis*-vacant pyrophyllite, cation migration must occur. The energy required for this accounts for the higher dehydroxylation temperature of *cis*-vacant pyrophyllite, as compared to *trans*-vacant pyrophyllite. The different dehydroxylation behavior of the two isomers originates from the fact that in *cis*-vacant pyrophyllite adjacent hydroxyl groups bridge different pairs of aluminum atoms, while in *trans*-vacant pyrophyllite they bridge the same pair. These conclusions are thought to be valid for other aluminous, 2:1-layer-type dioctahedral clay minerals.

Acknowledgment. We are grateful to HEFCE (United Kingdom) for funding the purchase of our Silicon Graphics Onyx2 machine under the JREI scheme. In addition, access to the Origin3800 machine at the U.K. national high performance computing service, CSAR, University of Manchester, was made possible through EPSRC grant no. GR/30907. The Ph.D studentship of S.S. was funded by Queen Mary, University of London, and W. R. Grace & Co. We are indebted to Dr Pascal Boulet for useful discussions.

References and Notes

(1) Fajnor, V. Š.; Kuchta, L. *J. Therm. Anal.* **1995**, *45*, 481.
(2) Fajnor, V. Š.; Jesenák K. *J. Therm. Anal.* **1996**, *46*, 489.
(3) Wang, L.; Zhang, M.; Redfern, S. A. T.; Zhang Z. *Clays Clay Miner.* **2002**, *50*, 272.
(4) Drits, V. A.; Besson, G.; Muller, F. *Clays Clay Miner.* **1995**, *43*, 718.
(5) Muller, F.; Drits, V.; Plançon, A.; Robert, J.-L. *Clays Clay Miner.* **2000**, *48*, 572.
(6) Frost, R. L.; Barron, P. F. *J. Phys. Chem.* **1984**, *88*, 6206.
(7) Fitzgerald, J. J.; Dec, S. F.; Hamza, A. I. *Am. Mineral.* **1989**, *74*, 1405.
(8) Fitzgerald, J. J.; Hamza, A. I.; Dec, S. F.; Bronnimann, C. E. *J. Phys. Chem.* **1996**, *100*, 17351.
(9) Tennakoon, D. T. B.; Thomas, J. M.; Jones, W.; Carpenter, T. A.; Ramdas, S. *J. Chem. Soc., Faraday Trans. 1* **1986**, *82*, 545.
(10) Guggenheim, S.; van Groos, A. F. K. *J. Therm. Anal.* **1992**, *38*, 2529.
(11) Bujdák, J.; Slosiariková, H. *J. Therm. Anal.* **1994**, *41*, 825.
(12) Bray, H. J.; Redfern, S. A. T. *Mineral. Magn.* **1998**, *62*, 647.
(13) Bray, H. J.; Redfern, S. A. T. *Mineral. Magn.* **2000**, *64*, 337.
(14) Sarikaya, Y.; Önal, M.; Baran, B.; Alemdaroglu, T. *Clays Clay Miner.* **2000**, *48*, 557.
(15) Emmerich, K.; Madsen, F. T.; Kahr, G. *Clays Clay Miner.* **1999**, *47*, 591.
(16) Emmerich, K. *Clays Clay Miner.* **2000**, *48*, 405.
(17) Emmerich, K.; Kahr, G. *Appl. Clay Sci.* **2001**, *20*, 119.
(18) Emmerich, K.; Plötze, M.; Kahr, G. *Appl. Clay Sci.* **2001**, *19*, 143.
(19) Tsipursky, S. I.; Drits, V. A. *Clay Miner.* **1984**, *19*, 177.
(20) Stackhouse, S.; Coveney, P. V.; Sandré, E. *J. Am. Chem. Soc.* **2001**, *123*, 11764.
(21) *CPMD*; Copyright IBM Corp. 1990−2001. Copyright MPI for Festkörperforschung, Stuttgart, 1997−2001.
(22) Payne, M. C.; Teter, M. P.; Allan, D. C.; Arias, T. A.; Joannopoulos, J. D. *Rev. Mod. Phys.* **1992**, *64*, 1045.
(23) Becke, A. D. *Phys. Rev. A* **1988**, *38*, 3098.
(24) Lee, C. T.; Yang, W. T.; Parr, P. G. *Phys. Rev. B* **1988**, *37*, 785.
(25) Tuckerman, M. E.; Martyna G. J. *J. Phys. Chem. B* **2000**, *104*, 159.
(26) Hutter, J.; Lüthi, H. P.; Parrinello, M. *Comput. Mater. Sci.* **1994**, *2*, 244.
(27) Fletcher, R. *Practical Methods of Optimization*; Wiley: New York, 1980.
(28) Grant, G. H.; Richards, W. G. *Computational Chemistry*; Oxford University Press: Oxford, 1985.
(29) Silvestrelli, P. L.; Parrinello, M. *J. Chem. Phys.* **1999**, *111*, 3572.
(30) Wardle, R.; Brindley, G. W. *Am. Mineral*, **1972**, *57*, 732.